Available online at www.sciencedirect.com
SCIENCE DIRECT®
Journal of Electroanalytical Chemistry 562 (2004) 95–103
Journal of Electroanalytical Chemistry
www.elsevier.com/locate/jelechem

Electropolymerization and doping/dedoping properties of polyaniline thin films as studied by electrochemical-surface plasmon spectroscopy and by the quartz crystal microbalance

Akira Baba [a], Shengjun Tian [a], Fernando Stefani [a], Chuanjun Xia [b], Zhehui Wang [a], Rigoberto C. Advincula [b], Diethelm Johannsmann [c], Wolfgang Knoll [a,*]

[a] *Max-Planck-Institute for Polymer Research, Ackermannweg 10, Mainz D-55128, Germany*
[b] *Department of Chemistry, University of Houston, Houston, TX 77204, USA*
[c] *Institute of Physical Chemistry, Technical University Clausthal, Arnord-Sommerfeld-Str. 4, Clausthal-Zellerfeld D-38678, Germany*

Received 6 March 2003; received in revised form 3 August 2003; accepted 20 August 2003

Abstract

The electropolymerization and doping/dedoping properties of polyaniline ultrathin films on Au electrode surfaces were investigated by a combination of in situ electrochemical techniques, i.e., electrochemical surface plasmon spectroscopy (ESPR) and the electrochemical quartz crystal microbalance (EQCM). In the ESPR measurements, we employed two wavelengths, i.e., 632.8 and 1152 nm in order to distinguish independently the electrochromic behavior. In addition, we used spectroelectrochemical transmittance measurements in order to probe further the optical properties of the polymer films as a function of the applied potential. The real and imaginary parts of the dielectric constant of the polyaniline thin film at several doping levels was determined quantitatively by taking into consideration the thickness values obtained from the EQCM measurement. The combination of these two techniques provides a powerful method for probing the electrical, optical, and dielectric properties of conjugated ultrathin polymer films.

Keywords: Surface plasmons; Quartz crystal microbalance; Polyaniline thin film; Doping/de-doping; Electrochromism; Complex dielectric constant

1. Introduction

The electrochemical and optical quantitative analysis of π-conjugated polymer ultrathin films upon oxidation/reduction and doping/dedoping is of great interest to a number of applications. This includes electrochromic displays [1], battery electrodes [2], sensors, and others. Because of the many factors affecting the transition between the doped and dedoped states of these polymer films, it is very difficult to obtain the quantitative analysis of each electrochemical event. A number of experimental in situ techniques on the doping/dedoping process of conjugated polymers has been introduced such as the quartz crystal microbalance (QCM) [3,4], FTIR [5], scanning probe microscopy (SPM) [6], etc.

Surface plasmon resonance (SPR) spectroscopy has become a widely accepted method for the characterization and study of ultrathin films, interfaces and kinetic processes at surfaces [7]. The combination of SPR with electrochemical measurements has been demonstrated as a powerful technique for the simultaneous characterization and manipulation of electrode/electrolyte interfaces [8–10]. With electrochemical-SPR measurements, the gold substrate that carries the optical surface mode is simultaneously used as the working electrode in the electrochemical experiments. One advantage of using the ESPR technique is that the electrochemical and optical properties are obtained *simultaneously* from films on the nanometer thickness

* Corresponding author. Tel.: +49-6131-379-160; fax: +49-6131-379-100.
E-mail address: knoll@mpip-mainz.mpg.de (W. Knoll).

0022-0728/$ - see front matter © 2003 Elsevier B.V. All rights reserved.
doi:10.1016/j.jelechem.2003.08.012

scale. Recently, the ESPR technique has been applied also for the characterization of a variety of conducting polymer films [11–17]. This involved the in situ monitoring of the film swelling/shrinking and the electrochromic properties during electropolymerization or anion doping/de-doping. The ESPR technique has also been combined with surface plasmon field enhanced light scattering (SPFELS) and the quartz crystal microbalance (QCM) technique for the characterization of conducting polymer films. A first attempt to combine the QCM/SPR [17] with electrochemical measurements was recently reported by Bailey et al. [18] Attempts to combine SPR/SPFELS with the electropolymerization of conducting polymers have also been recently described by our group [12,13]. We investigated the electrochemical process of polyaniline using the combined technique to obtain information on the morphological transition corresponding to the electrochemical and dielectric properties during in-situ electropolymerization.

Polyaniline (PANI) has been known and studied extensively since the 1980s [19]. The interest in this material and its derivatives is mainly due to its interesting electrical and optical properties together with its chemical tunability, ease of derivatization, solubility in a variety of solvents, processability into fibers and films, and its stability. During the past two decades, the chemical and physical properties of polyaniline have been studied extensively under different conditions and, together with polypyrrole, this material has become one of the most popular conducting polymers. A complete review of the tremendous advances in the chemistry, electrochemistry, physics, theory, and processing of polyaniline has been given by MacDiarmid [20]. Polyaniline has three main stable oxidation states: the fully reduced ''leucoemeraldine'' form, the 50% oxidized ''emeraldine'' form, and the fully oxidized ''pernigraniline'' form. Each of these can exist in the form of its base or in the form of its protonated (doped) salt. Oxidative doping of the ''leucoemeraldine'' or protonic acid doping of the ''emeraldine'' produces the conducting form, with an increase in conductivity, which can reach up to 10 orders of magnitude; the conductivity of the emeraldine salt can vary between 0.5 and 400 S/cm depending on the preparation [21].

In this study, the quantitative analysis of an ultrathin polyaniline film during the oxidation/reduction and the doping/dedoping cycles is reported using ESPR and EQCM techniques. First, the electropolymerization process is investigated. The deposition process as monitored by the QCM allowed for the determination of the amount of charge transferred to each monomer during the electropolymerization. The SPR reflectivity curve during the electropolymerization strongly depends on the dielectric constant of the deposited polyaniline film. Upon oxidation and reduction and upon doping and dedoping, the polyaniline films undergo a substantial increase and decrease, respectively, in conductivity. These changes occur simultaneously with significant changes in the dielectric constants and the thickness of the films and hence, their optical behavior as probed by SPR and QCM. The film properties, i.e., thickness, real part, and imaginary part of the dielectric constant upon doping/dedoping could be determined quantitatively by these techniques.

2. Experimental

2.1. Materials

Aniline and sulfuric acid were purchased and used as received from Aldrich and Riedel-de Haën, respectively.

2.2. Electrochemistry

All potentiostatic and cyclic voltammetry measurements were carried out using a one-compartment, three-electrode cell driven by an EG & G PAR potentiostat (Model 263A). In all the measurements, the working electrodes consisted of gold films ($d \sim 50$ nm) vacuum evaporated unto an LaSFN9 glass substrate (with an adhesion layer of 2 nm Cr, previously evaporated on glass). The counter electrode was a platinum wire and the reference an Ag|AgCl 3 M NaCl aqueous electrode. All the potentials reported in this paper are relative to this reference electrode. The solutions were carefully purged with nitrogen.

2.3. Electrochemical-surface plasmon resonance spectroscopy (ESPR) measurement

The SPR set-up combines the three-electrode electrochemical cell with a Kretschmann configuration for the excitation of surface plasmons. Details of this set-up can be found elsewhere [22]. Surface plasmons are excited by reflecting p-polarized laser light off the Au-coated base of the prism. The excitation sources employed were two different He–Ne lasers: $\lambda = 632.8$ and 1152 nm. Kinetic measurements were performed in order to monitor the formation of the polyaniline film and the oxidation/reduction and doping/dedoping properties of the deposited polyaniline thin film via reflectivity changes as a function of time. Angular measurements were also performed by scanning an incident angle range while the potential was held constant. For these experiments, the gold film thickness was chosen for optimum excitation of the surface plasmons with both wavelengths (42–45 nm). The electrode surface area was 0.785 cm^2.

2.4. Electrochemical-quartz crystal microbalance (EQCM) measurement

Commercial 5 MHz AT-cut quartz crystals with Au electrodes and a crystal holder (Maxtek Inc., USA) were used. The front electrode of the crystal was used as the working area and the back electrode was grounded, and both electrodes were connected at the back side to an impedance analyzer. On both sides of the crystal, O-rings were used to prevent leakage. Details concerning this set-up can be found elsewhere [23]. The crystals were plasma cleaned before measurement. An impedance analyzer (HP E5100A, 10 kHz–300 MHz, Agilent Technologies) was used in the measurement. From the impedance analysis, both the shift in frequency and the change in the half-band-half width (HBHW) are obtained from fits of the resonance curves to the conductance spectra. The latter quantity is related to dissipation. In order to separate the rf voltage (network analyzer) and the dc voltage (potentiostat), a combination of a capacitor and an inductance was used as described elsewhere [24]. In EQCM, the electrode surface area was determined to be 1.33 cm^2.

2.5. Transmittance measurement

In order to complement the information obtained by the ESPR and the EQCM experiments, transmittance measurements were carried out with both lasers during the potential cycling (cyclic voltammetry), between −0.2 and 0.9 V at a scan rate of 20 mV/s. In this case, the gold film thickness was reduced to 20 nm to allow transmission measurements on the glass substrates.

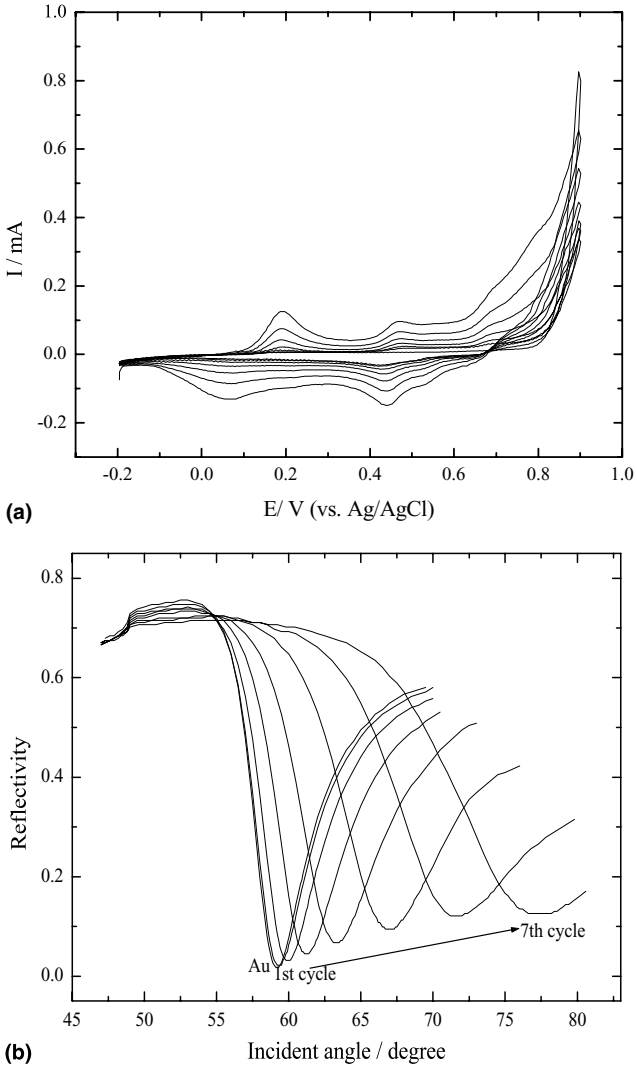

Fig. 1. (a) Cyclic voltammogram of the electropolymerization of aniline (0.02 M) in H_2SO_4 (0.5 M) solution and (b) angular SPR reflectivity curve measured after each potential cycle.

3. Results and discussion

3.1. Electropolymerization of aniline

Electrochemical polymerization of aniline on the gold surface was achieved by applying potential cycling between −0.2 and 0.9 V at a scan rate of 20 mV/s. The cyclic voltammogram (CV) obtained during the electropolymerization is shown in Fig. 1a up to the seventh cycle. Similar conditions in aqueous H_2SO_4 for the potential range described, has been used by many groups [25–30]. As reported previously, the first redox process (ca. 0.22 V in the positive scan and 0.05 V in the negative scan) corresponds to the electron transfer from/to the electrodeposited polyaniline film. In order to compensate the charge of the polyaniline film, anion transport from/to the electrolyte solution, i.e., anion doping and dedoping [31,32], should occur. This phenomenon is responsible for the dramatic change in the conductivity of the PANI film. The electrodeposition of polyaniline on the Au electrode proceeds via a radical cation mechanism. The second redox process (ca. 0.5 and 0.45 V, for the oxidation and reduction, respectively) probably corresponds to side reactions such as decomposition of the polymer. The large currents observed at the positive end of the CV are due to the superposition of two distinct processes: one is the electron transfer from the PANI film corresponding to the oxidation of the PANI film [33] and the other is the electron transfer from the aniline monomer to the electrode corresponding to the oxidation of the aniline monomer to produce a precursor for the PANI film. A series of angular SPR curves taken after each potential cycle are shown in Fig. 1b. These scans were measured in the solution at open circuit potential (ocp $\approx$ 0.15 V). Shifts of the dip angles in the SPR curves were observed indicating that

polyaniline was deposited onto the gold film electrode during each potential cycle.

The in situ formation of the PANI film on the gold electrode surface was monitored by the measurement of the charge transferred, by QCM and by SPR. Fig. 2 shows the complex frequency change during electropolymerization by cycling the potential between −0.2 and 0.9 V at a scan rate of 20 mV/s. Each arrow shows the starting point of each potential cycle, i.e., −0.2 V. In the QCM measurements, the Sauerbrey-approximation was used for the analysis of the frequency shifts, stating that the frequency shift is mostly caused by deposition of mass on the crystal surface. Thus one obtains: $\Delta f/f \approx -\Delta m/m_q = -\Delta m\ 2f_0/Z_q$, with Δf the frequency shift, f the frequency, f_0 the fundamental frequency, Δm the change in areal mass density for the film, $m_q = Z_q/(2f_0)$ the areal mass density of the quartz plate, and $Z_q = 8.8 \times 10^6$ kg m^{-2} s^{-1} the acoustic impedance of the AT-cut quartz crystal. The Sauerbrey approximation does not account for viscous losses or viscoelastic effects. In air, such viscoelastic effects scale as the cube of the film thickness and can be neglected. In liquids this is not the case. Because the liquid exerts a lateral stress onto the moving upper surface of the film, there are viscoelastic effects which scale *linearly* with the mass. This leads to a modified Sauerbrey equation, which is [23,24]

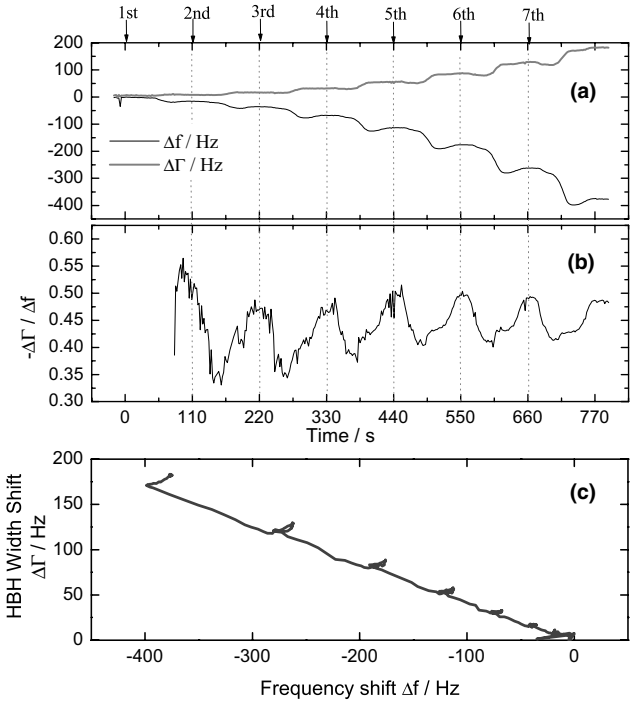

Fig. 2. In situ monitoring of complex frequency change (a), $\Delta\Gamma/\Delta f$ plot (b) as a function of time, and $\Delta\Gamma$–Δf plot (c) during electropolymerization of aniline by potential cycling between −0.2 and 0.9 V at a scan rate of 20 mV/s.

$$\begin{aligned}\frac{\Delta f + \mathrm{i}\Delta\Gamma}{f} &\approx -\frac{\Delta m}{m_q}\left\{1 - \left(\frac{Z_q^2}{Z_f^2} - 1\right)\frac{2\pi\mathrm{i} f \rho_l \eta_l}{Z_q^2}\right\} \\ &\approx -\frac{\Delta m}{m_q}\left\{1 - \frac{2\pi\mathrm{i} f \rho_l \eta_l}{Z_f^2}\right\} \\ &= -\frac{\Delta m}{m_q}\left\{1 - J_f \frac{2\pi\mathrm{i} f \rho_l \eta_l}{\rho_f}\right\}, \end{aligned} \quad (1)$$

where ρ_l is the density of the liquid, η_l is the viscosity of the liquid, Z_f is the acoustic impedance of the film, ρ_f is the density of the film, and $J_f = J_f' - \mathrm{i}J_f''$ is the complex compliance of the film. In the second line the relation $Z_q \gg Z_f$ (film is softer than quartz plate) has been used. Note that the above expression is only the first term of a Taylor expansion in the film mass Δm. More complicated equations apply for films with a thickness comparable to the wavelength of sound [34]. For the analysis of conventional QCM data, the above equation is of limited use because it does not allow for a separation of mass effects and viscoelastic effects (the second term in the curly brackets). One defines a "Sauerbrey mass" which is the true mass times the unknown correction factor in curly brackets. If, on the other hand, the bandwidth (HBHW) is available, it can be interpreted in the frame of this equation. The ratio of $\Delta\Gamma$ and $-\Delta f$ should be independent of mass. This is indeed the case for our data, as shown in Fig. 2(c). The quantity $-\Delta\Gamma/\Delta f$ corresponds to the ratio of the imaginary and the real part of the curly bracket, namely

$$\frac{-\Delta\Gamma}{\Delta f} \approx \frac{J_f'}{\rho_f/(2\pi f \rho_l \eta_l) - J_f''}. \quad (2)$$

The above equation allows for some further conclusions. Assuming $\rho_f \approx \rho_l$ the first term in the denominator is of the order of the viscous compliance of the liquid. Further assuming that the liquid is much softer than the film, $J_f'' \ll 1/(2\pi f \eta)$ (a safe assumption for most polymeric films) one reaches the conclusion

$$\frac{\Delta\Gamma}{\Delta f} \approx J_f'(2\pi f \eta_l) \approx J_f'/[30\ \mathrm{MPa}^{-1}], \quad (3)$$

where $\eta_l \approx 10^{-3}$ Pa s and $f = 5 \times 10^6$ has been used in the second line. The quantity $-\Delta\Gamma/\Delta f$ therefore provides a measure of the elastic compliance of the films. Note that this interpretation contradicts simple intuition to some degree: while one would naively associate a shift in bandwidth to a dissipation inside a film (given by J'', the detailed derivation shows that it is actually the *elastic* compliance, J', which is measured.

Again, in liquids a *modified* Sauerbrey equation holds, which is different from the dry case in two respects: first, the mass, Δm includes the trapped liquid. Second, there are viscoelastic corrections as given by the curly bracket in Eq. (1). As for the frequency shift,

nothing can be learned because the elastic correction is inseparable from the effect of the (unknown) mass. One can, however, extract information from the bandwidth. Making some assumptions, the bandwidth can be used to estimate the elastic compliance, J', of the film.

The application of this formalism to our data is illustrated in this Figure. Fig. 2(a) shows the raw data. $-\Delta f$ and $\Delta\Gamma$ mostly go in parallel, but not quite. During every positive scan, the ratio $-\Delta\Gamma/\Delta f$ drops slightly (Fig. 2(b)). During every negative scan, it increases again. This behavior is largely independent of thickness (Fig. 2(c), the "D–f-plot", where "D" stands for "dissipation"). The above quantitative discussion suggests that the (average) elastic compliance of the film is in the range of 10 MPa. It drops slightly during a positive scan and recovers during a negative scan. One possibility for this is that the PANI film becomes more porous by dedoping but recovers by doping. Shown in Fig. 3(a) are the mass change as a function of time during the seven electropolymerization cycles and corresponding SPR minimum angle shifts measured after each potential cycle. Each arrow shows the starting point of each potential cycle, i.e. −0.2 V. In observing the mass change, the increase in each of the cycles mostly corresponds to the oxidation of aniline to form the polyaniline film and the doping of anions into the deposited polyaniline film. The decrease of the curve is mostly due to the dedoping of the anions from the deposited polyaniline film. The trace of the SPR minimum angle shift was similar to the mass change at −0.2 V, i.e., at the end of each potential cycle. This indicates that the optical thickness corresponds to the acoustic mass. The kinetic measurements for SPR were performed at a fixed angle, 58.0° slightly below the angle of the reflectivity minimum (see Fig. 1(b)) of the blank gold substrate as shown in Fig. 3(b). In the kinetic measurement, the behavior of the reflectivity shows a large difference with mass change. In the case of the SPR reflectivity, the curve is very sensitive to the thickness, the real (ε') and the imaginary (ε'') parts of the dielectric constant. The increase in reflectivity below about +0.2 V was seen in the figure whereas no increase was observed in the mass. This clearly indicates that the dielectric constant changes dramatically in this potential range (−0.2 to +0.2 V). Fig. 3(c) shows the current efficiency, $\Delta m/\Delta Q$ during the electropolymerization process. From this plot, it was found that the current efficiency increases with time. This property is also seen in the change of the mass as a function of charge transferred as shown in the inset. In EQCM measurements, the areal mass density m_f during electropolymerization is related to the charge density passed Q, on the other hand, it also contributes to the generation of solute oligomer [24]. In the case of electropolymerization for the conducting polymer, the theoretical value of the current efficiency, m_f/Q is calculated from,

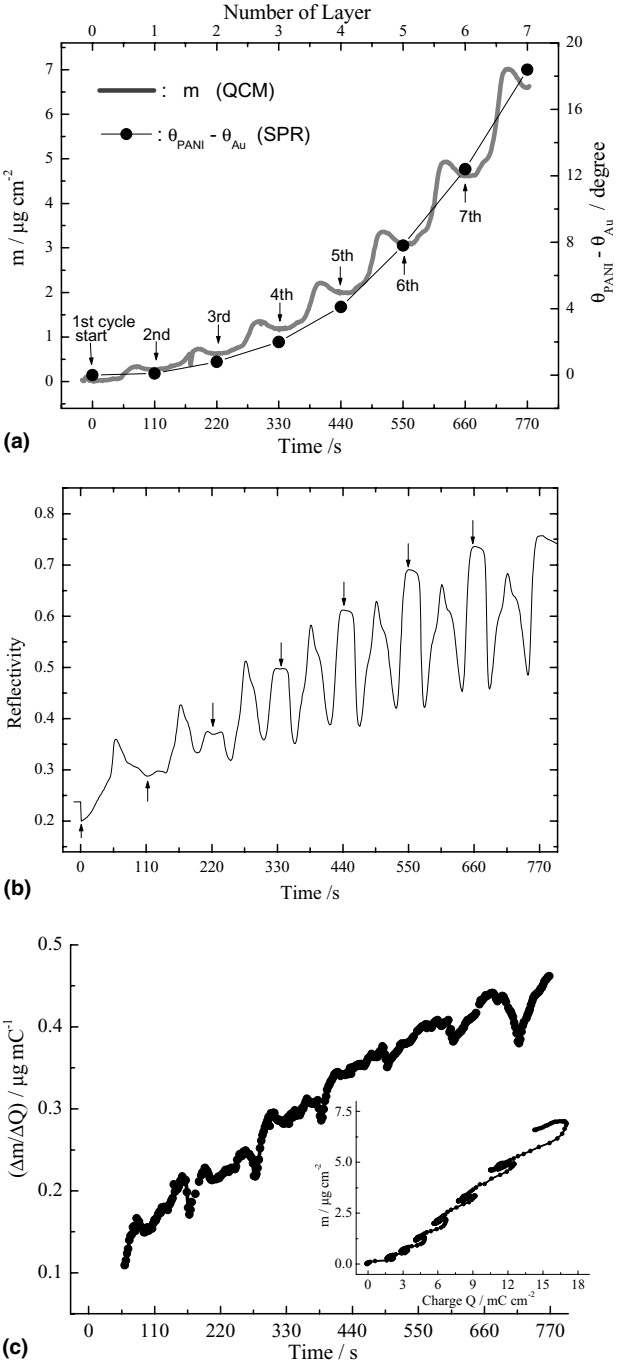

Fig. 3. In situ monitoring of mass change during electropolymerization of aniline by potential cycling between −0.2 and 0.9 V at a scan rate of 20 mV/s, and corresponding SPR minimum angle shifts measured after each potential cycle (a). The reflectivity as a function of time during the electropolymerization (b). A current efficiency $\Delta m/\Delta Q$ plot during electropolymerization (c). Inset is the mass change as a function of charge amount.

$$\frac{m_f}{Q} = \frac{(M_M - 2M_H) + x_A M_A}{(2 + x_A)F}, \tag{4}$$

where M_M, M_A, and M_H are the molar masses of the monomer, the incorporated anion, and hydrogen. The

quantity x_A is the doping level equal to the ratio of the number of moles of inserted anion to that of monomer group in the film. F is the Faraday constant, 96 485 C mol^{-1}. The incorporation of water molecules and neutral salts which can cause apparently higher $\Delta m/\Delta Q$ values, were not included in this model. Assuming $x_A = 0.4$, the theoretical current efficiency $\Delta m/\Delta Q$ is expected to be 0.952 μg/mC. As shown in Fig. 3(c), the value found experimentally, was at first, much smaller than the theoretical value, and then finally was much larger (the ratio of experimentally determined $\Delta m/\Delta Q_{exp}$/theoretical current efficiency $\Delta m/\Delta Q_{theo}$: 48.6 % after seven cycles) than for the initial potential cycles of electropolymerization (17.3% after 1 cycle). This indicates that a number of side reactions, which do not correspond to a mass increase, e.g., the formation of oligomers, accompany the ultrathin film formation [6].

3.2. Doping/dedoping properties of deposited polyaniline thin films in monomer-free solution

3.2.1. During potential cycling

The cyclic voltammetry curve of a deposited PANI film in monomer-free solution is shown in Fig. 4(a). The cyclic voltammetry was scanned between −0.2 and 0.9 V at a scan rate of 20 mV/s in a monomer-free 0.5 M H_2SO_4 solution. As mentioned before, the first redox peak (A, A′) is commonly assumed to correspond to the electron transfer from/to the PANI film. In order to compensate the charge of the PANI film, anion doping/dedoping of the polyaniline film occurs. This is also seen in the EQCM measurement in which the mass increase at around 0.2 V corresponds to this doping process. The second redox peak (B, B′) corresponds to a deprotonation and protonation process. Besides the proton/cation exchange, the anion is also expelled from the polyaniline film during deprotanation [3]. The small peak at around 0.5 V is probably due to a side reaction in the polyaniline film.

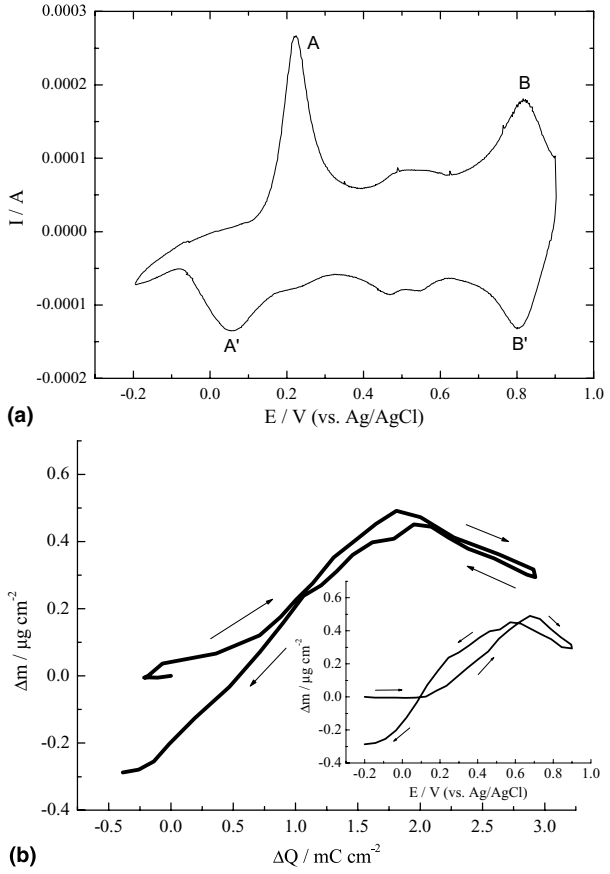

Fig. 4. (a) Cyclic voltammetry of deposited polyaniline film in monomer-free solution and (b) its mass response as a function of charge amount (second cycle). Inset is the mass response as a function of potential.

If one correlates the deposited mass with the transferred charge (Fig. 4(b)), first, the mass increased with the amount of charge transferred and then decreased again. The $\Delta m/\Delta Q$ value in this region is 0.27 μg/mC. This value is smaller than the theoretical $\Delta m/\Delta Q$ value of SO_4^{2-} (0.50 μg/mC). This might be due to the participation of protons in the charge compensation. At around 1.8 mC/cm^{-2} (0.7 V), the mass started to decrease again. The $\Delta m/\Delta Q$ value in this region is 0.18 mC/cm^{-2}. This should be attributed to a combination of protonation, anion de-doping, and degradation [35,36]. The degradation could result in a mass loss after potential cycling as seen in this figure. In our QCM experiments, a mass loss of 60% of the deposited polyaniline film was observed after 10 potential cycles between −0.2 and 0.9 V (cf. also Fig. 7).

In the transmission measurements, the decrease of the transmitted intensity begins at around 0.1 V for both wavelengths, $\lambda = 632.8$ and 1152 nm as shown in Fig. 5. These wavelengths were intentionally chosen in order to compare with ESPR results discussed later. As can be seen from the Fresnel algorithm calculations, the transmitted intensity depends mostly on the imaginary part (ε'') of the dielectric constant of the deposited polyaniline film. The absorption around 632.8 nm is generally attributed to the exciton absorption of the quinoid ring structures [37–40]. Therefore, the decrease at around 0.1 V shows the oxidation of the polyaniline film from its leucoemeraldine to its emeraldine state, which contains quinoid ring structures. The absorption in the near infrared (NIR) region is known to be due to free charge carriers in a highly conductive state [41–43]. At the first oxidation peak, the polyaniline film changes to the "emeraldine" form from the "leucoemeraldine" form. This "emeraldine" form is protonated in the acid solution so that it has a high conductivity. At the second oxidation peak, the polyaniline film is changed to the "pernigraniline" state from the "emeraldine" form and is deprotonated so that it is not highly conductive.

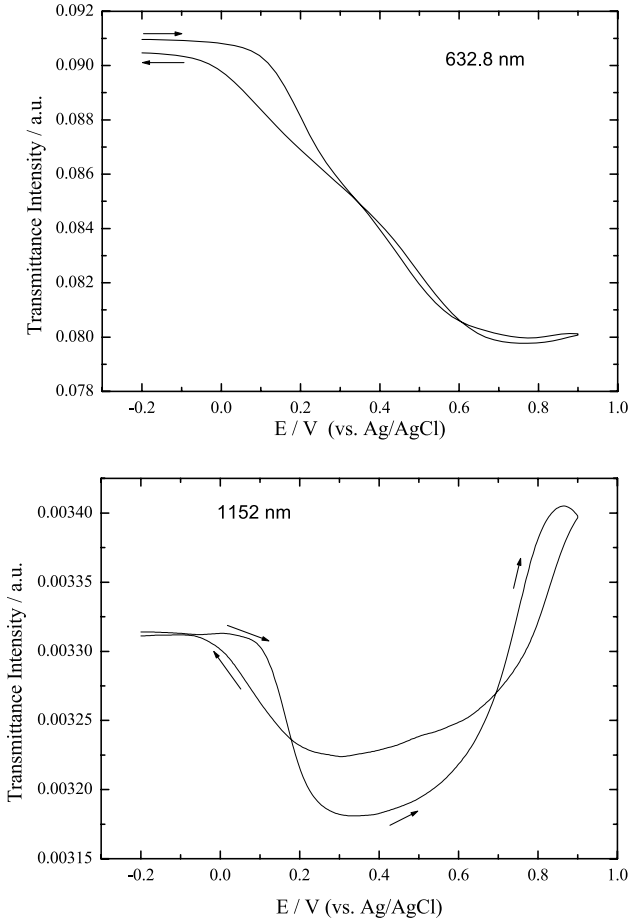

Fig. 5. Transmittance intensity response at 632.8 and 1152 nm during potential cycling in monomer-free solution.

3.2.2. Potentiostatic measurements

In the previous section, a qualitative analysis of the imaginary part of the dielectric constant could be given for the three states of the polyaniline film. In order to be quantitative to all parameters of the films, i.e., its thickness, and the real and imaginary part of dielectric constant, we used ESPR and EQCM data taken under potentiostatic measurement conditions. In Fig. 6, the potentiostatic SPR scans are shown for both $\lambda = 632.8$ and 1152 nm, respectively. All SPR angular scans were started after each potential was applied for 2 min in order to have the same conditions as in the QCM measurements. Some very interesting information was obtained from the analysis of these curves. First, it is noticeable that the change in the reflectivity curves at around 0.2 V occurs when the polyaniline "base" film changes, upon doping, into the corresponding conducting polyaniline salt. This process is reversible and many cycles can be performed without any noticeable variation (except for any degradation processes). If the film, in the absence of monomers, is kept at 0.9 V, the SPR behavior is again likened to that of the insulating state and subsequent SPR scans at 0.65, 0.4, −0.2, 0.4,

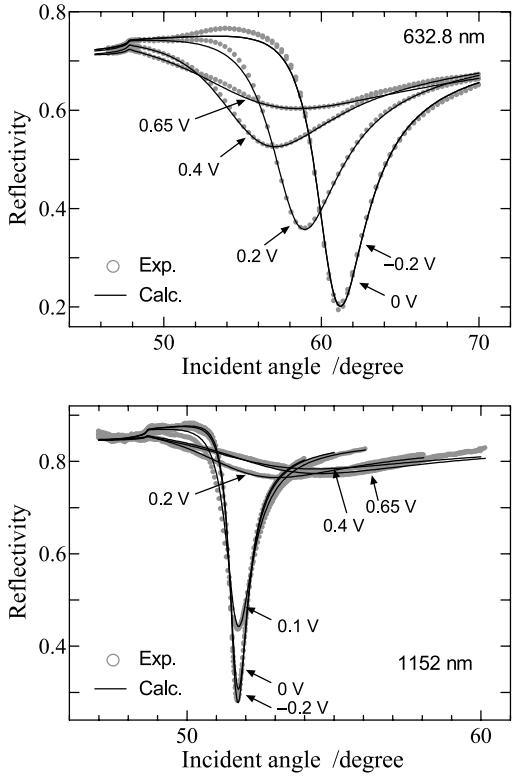

Fig. 6. Experimental angular SPR reflectivity curve (dotted) and calculated curve (solid) under applied potential at 632.8 and 1152 nm.

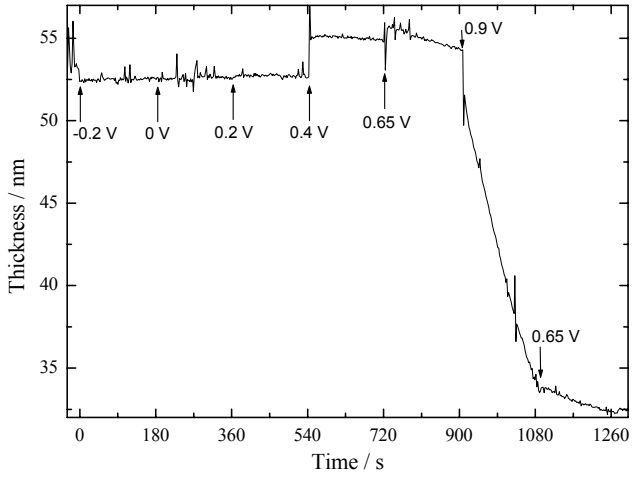

Fig. 7. Thickness change measured by QCM under potential applied.

and 0.65 V showed no difference. This indicates that in the absence of the aniline monomer, oxidation at potentials higher than ca. 0.65 V leads to an irreversible degradation of the electrochemical response of the polyaniline film.

Since it is difficult to obtain independent information on the thickness and the real and imaginary parts of the dielectric constant from mere SPR measurement, we also used the QCM in a potentiostatic mode of the measurement. As explained before, the Sauerbrey equation [44] could be applied to relate frequency shifts

to mass changes. Fig. 7 shows the potentiostatic QCM measurements for several potentials and the corresponding thickness, roughly estimated on the assumption of a mass density of 1.3 g/cm^3 [45] for comparison with the ESPR results. For changing the potential, a step potential program was used. In contrast to the SPR reflectivity curves, which show a large change at 0.2 V, the thickness from the QCM measurement was found to be roughly constant between −0.2 and 0.2 V. As can be seen from Fig. 7, a substantial degradation and loss of material sets in at 0.9 V so that one cannot obtain a meaningful film thickness at 0.9 V. The loss of film thickness at 0.9 V was found to be 38 % after 3 min. Fitting the experimental SPR reflectivity results with the thickness values obtained from QCM measurement (except the value of 0.9 V) gives the theoretical reflectivity curves that are also shown in Fig. 6. The calculation was done by using Fresnel's equations for a Prism/Cr/Au/PANI/electrolyte solution architecture. Details for the fitting procedure can be found elsewhere [7]. Although the SP resonance at $\lambda = 1152$ nm is very broad at high potential, excellent fitting curves were obtained in most cases. The fitting parameters obtained are shown in Fig. 8. Dramatic changes both in the real part and the imaginary part of the dielectric constants were determined at both wavelengths. The trends of changes in the imaginary part at both wavelengths coincide well with the transmittance measurements shown in Fig. 5. The error bars in Fig. 8 are based on the density fluctuation of the polymer upon doping/de-doping, that is 1.25–1.35. Based on these calculations, the accuracy for the determination of the complex dielectric constant is estimated to be better than ±0.02 for the real part and ±0.10 for the imaginary part of the dielectric constant in this density range, i.e., ESPR measurements are able to determine the complex dielectric constants of the conducting polymer films in the doped/de-doped state rather independently of the uncertainty in the film density. Thus, the electrochromic phenomena of PANI films can be characterized by this ESPR technique with high sensitivity, which may lead to new designs for SPR-based sensors/biosensors based on the electrochromism of thin conducting polymer films. Similar experiments are currently underway with other conducting polymers such as poly(3,4-ethylenedioxythiophene) (PEDOT).

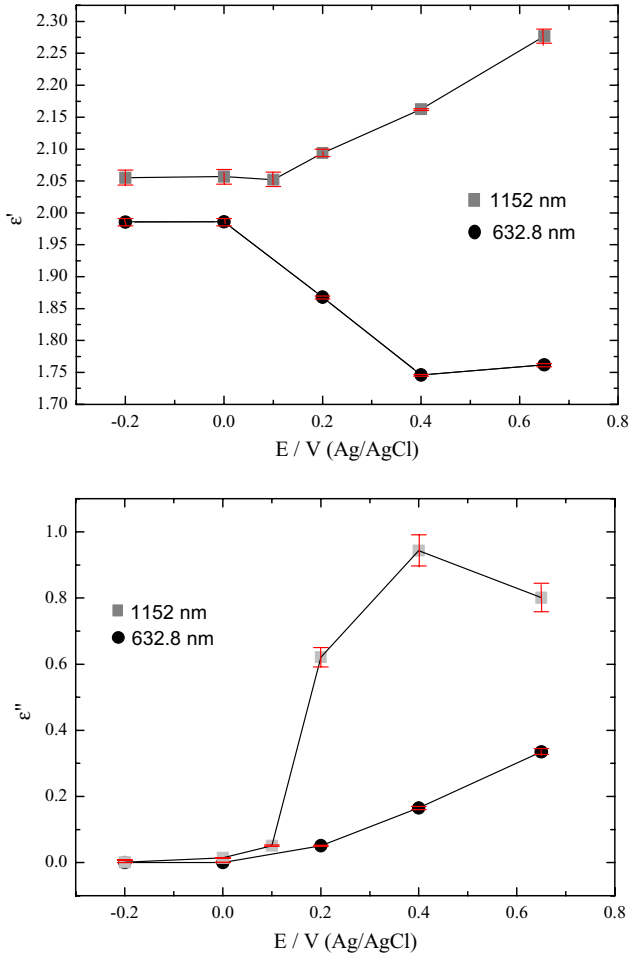

Fig. 8. Real part (ε') and imaginary part (ε'') of the dielectric constants at several potentials.

4. Conclusions

Using the combined electrochemical-surface plasmon resonance spectroscopy (ESPR) and the electrochemical-quartz crystal microbalance (EQCM) techniques, it was possible to monitor quantitatively the electropolymerization and doping/dedoping properties of polyaniline films on a flat gold substrate surface. Transmittance and potentiostatic SPR measurements were carried out with two wavelengths in order to obtain independent information about the electrochromic properties of the thin polayaniline film. The change in the electrochemical/optical properties of the thin film upon doping produces a dramatic change in the SPR response primarily due to a distinct change in the real and imaginary parts of the dielectric constant. The contribution of the thickness is roughly estimated independently by EQCM measurements. Thus, using these experimental combinations, we have demonstrated the ability to obtain independent quantitative values on the thickness and the real and imaginary parts of the dielectric constant at two wavelengths. These techniques should be a powerful combination for the quantitative analysis of other conjugated polymer ultrathin films.

Acknowledgements

We thank Dr. Andreas Bund (Dresden University of Technology), Dr. Jörn Lübben, and Dr. Kaoru Tamada

(AIST, Tsukuba) for helpful discussions and Dr. Steffen Berg for experimental help. A.B. acknowledges the Alexander von Humboldt Foundation and the Max-Planck-Society for a postdoctoral fellowship.

References

[1] T. Kobayashi, H. Yoneyama, H. Tamura, J. Electroanal. Chem. 161 (1984) 419.
[2] A.G. MacDiarmid, S.L. Mu, N.L.D. Somarisi, W. Mu, Mol. Cryst. Liq. Cryst. 121 (1985) 187.
[3] D. Orata, D.A. Buttry, J. Am. Chem. Soc. 109 (1987) 3574.
[4] S.-Y. Cui, S.-M. Park, Synth. Met. 105 (1999) 91.
[5] A. Zimmermann, L. Dunsch, J. Mol. Struct. 410 (1997) 165.
[6] R. Nyffenegger, E. Ammann, H. Siegenthaler, O. Haas, Electrochim. Acta 40 (1995) 1411.
[7] W. Knoll, Annu. Rev. Phys. Chem. 49 (1998) 569.
[8] A. Tadjeddine, D.M. Kolb, R. Kötz, Surf. Sci. 101 (1980) 277.
[9] J.G. Gordon II, S. Ernst, Surf. Sci. 101 (1980) 499.
[10] Y. Iwasaki, T. Horiuchi, M. Morita, O. Niwa, Electroanalysis 9 (1997) 1239.
[11] A. Baba, R.C. Advincula, W. Knoll, in: D. Möbius, R. Miller, Novel Methods to Study Interfacial Layers, Studies in Interface Science, Elsevier Science, vol. 11, 2001, p. 55.
[12] A. Baba, R.C. Advincula, W. Knoll, J. Phys. Chem. B 106 (2002) 1581.
[13] A. Baba, M.-K. Park, R.C. Advincula, W. Knoll, Langmuir 18 (2002) 4648.
[14] C. Xia, R. Advincula, A. Baba, W. Knoll, Langmuir 18 (2002) 3555.
[15] V. Chegel, O. Raitman, E. Katz, R. Gabai, I. Willner, Chem. Commun. (2001) 883.
[16] X. Kang, Y. Jin, G. Chen, S. Dong, Langmuir 18 (2002) 1713.
[17] A. Laschitsch, B. Menges, D. Johannsmann, Appl. Phys. Lett. 77 (2000) 2252.
[18] L.E. Bailey, D. Kambhampati, K.K. Kanazawa, W. Knoll, C.W. Frank, Langmuir 18 (2002) 479.
[19] A.G. MacDiarmid, J.C. Chiang, A.F. Richter, A.J. Epstein, Synth. Met. 18 (1987) 285.
[20] A.G. MacDiarmid, Synth. Met. 84 (1997) 27.
[21] Y. Cao, G.M. Treacy, P. Smith, A.J. Heeger, Appl. Phys. Lett. 60 (1992) 2711.
[22] E.F. Aust, S. Ito, M. Sawodny, W. Knoll, Trends Polym. Sci. 2 (1994) 9.
[23] D. Johannsmann, Macromol. Chem. Phys. 200 (1999) 501.
[24] A. Bund, G. Schwitzgebel, Electrochim. Acta 45 (2000) 3703.
[25] G. Zotti, S. Cattarin, N. Comisso, J. Electroanal. Chem. 239 (1988) 387.
[26] L. Duic, Z. Mandic, J. Electroanal. Chem. 335 (1992) 207.
[27] L. Duic, Z. Mandic, S. Kovac, Electrochim. Acta 40 (1995) 1681.
[28] K. Prasad, N. Munichandraiah, Synth. Met. 123 (2001) 459.
[29] K. Rajendra Prasad, N. Munichandraiahz, Electrochem. Solid-State Lett. 12 (2002) 271.
[30] D. Ljerka, M. Zoran, K. Franjo, J. Polym. Sci. 32 (1994) 105.
[31] S. Mu, C. Chen, J. Wang, Synth. Met. 88 (1997) 249.
[32] W.S. Huang, B.D. Humphrey, A.G. MacDiarmid, J. Chem. Soc. Faraday Trans. 1 (1986) 82.
[33] E.M. Genies, C.J. Tsintavis, J. Electroanal. Chem. 195 (1985) 109.
[34] D. Johannsmann, J. Appl. Phys. 89 (2001) 6356.
[35] L. Kwanghee, A.J. Heeger, Y. Cao, Synth. Met. 72 (1995) 25.
[36] T. Kobayashi, H. Yoneyama, H. Tamura, J. Electroanal. Chem. 177 (1984) 293.
[37] S. Stafstrom, J.L. Bredas, A.J. Epstein, H.S. Woo, D.B. Tanner, W.S. Huan, A.G. MacDiarmid, Phys. Rev. Lett. 59 (1987) 1464.
[38] A.A. Nekrasov, V.F. Ivanov, A.V. Vannikov, J. Eelctroanal. Chem. 482 (2000) 1.
[39] J. Stejskal, P. Kratochvil, N. Radhakrishnan, Synth. Met. 61 (1993) 225.
[40] D.E. Stilwell, S.-M. Park, J. Electrochem. Soc. 136 (1989) 427.
[41] Y. Min, Y. Xia, A.G. MacDiarmid, A. Epstein, J. Synth. Met. 69 (1995) 159.
[42] O.P. Dimitriev, N.V. Lavrik, Synth. Met. 90 (1997) 1.
[43] I. Kulszewicz-Bajer, Macromolecules 28 (1995) 610.
[44] G. Sauerbrey, Z. Phys. 155 (1959) 206.
[45] J. Stejskal, R.G. Gilbert, Pure Appl. Chem. 74 (2002) 857.